*D. M. Parks**

Three-Dimensional Aspects of HRR-Dominance

REFERENCE Parks, D. M., **Three-dimensional aspects of HRR-dominance**, *Defect Assessment in Components – Fundamentals and Applications*, ESIS/EGF9 (Edited by J. G. Blauel and K.-H. Schwalbe) 1991, Mechanical Engineering Publications, London, pp. 205–231.

ABSTRACT As crack fronts in power law hardening materials are approached, the asymptotic dominance of plane strain HRR singularity fields can provide a justification for one-parameter dominant singularity approaches to elastic–plastic fracture. Since HRR fields do not account for finite crack tip blunting, one can only hope that they accurately describe the fields in a small annular zone surrounding the tip. At large loads, growth of the blunting zone can 'push' the potential HRR zone so far from the crack front that single-parameter (e.g., J-based) descriptions no longer apply.

The eventual loss of J-dominance in two-dimensional plane strain crack configurations, including important effects of degree of strain hardening, crack geometry, and loading type and magnitude, are now fairly well understood. A recently proposed two-parameter characterisation of plane strain crack tip fields accurately and predictively describes the spectrum of observed fields ranging from HRR-type J-dominated ones to those exhibiting greatly diminished constraint and triaxiality. However, three-dimensional (3D) aspects of this process are less well documented. We summarise recent 3D finite element calculations and related experimental evidence on this topic for part-through surface-cracked plates and for through-cracked thin plates. Roughly speaking, local plane strain J-dominance can be lost along a 3D crack front due to interaction of the (otherwise ~ autonomous) crack tip fields with either the local *in-plane* or local *out-of-plane* parts of the global 3D fields in the cracked structure. Possible three-dimensional generalisations of a recently-proposed two-parameter description of plane strain crack tip fields are briefly discussed.

Introduction

The major contribution of fracture mechanics methodology has been the notion of correlating the crack extension behaviour of two different cracked bodies (e.g., laboratory specimens and engineering structures) based on the similarity (or not!) of their respective near crack tip stress and deformation fields. The degree of similarity is often assessed based solely on the strength of dominant singular asymptotic crack tip fields emerging from various constitutive and kinematical idealisations. Familiar examples of such parameters are the stress intensity factor, K_I, of linear elastic fracture mechanics (LEFM) and the J-integral of non-linear (elastic) fracture mechanics (NLEFM). Providing that such single-parameter asymptotic characterisations actually 'dominate', or control in a more or less one-to-one fashion, the complete near-crack-front fields in the zone of operative microfracture processes, the loading in either body can be scaled to give 'similar' local crack front fields. With the further assumption that the prospective crack front microfracture nuclei are 'similarly'

* Department of Mechanical Engineering, Massachusetts Institute of Technology, Cambridge, Massachusetts 02139, USA.

distributed and possess identical kinetics in the two bodies, we expect that the macroscopic crack extension behaviour in each body can be phenomenologically described in the same way. In particular, the J-based approach to the analysis of quasi-stationary cracks has proven to be an effective means of correlating the beginning of ductile cracking. For a recent review of this approach, see Hutchinson **(8)**.

The many successes of fracture mechanics attest to the general suitability of the crack-front-similarity/crack-extension correlation. However, there remain certain issues of concern. For example, in the vicinity of transition temperature, statistical aspects of cleavage fracture initiation can give rise to considerable scatter in macroscopic toughness even in 'identical' specimens. Secondly, the complex and varied nature of the elastic–plastic crack tip fields which have been observed in detailed finite element analyses has made the assessment of 'similarity' somewhat elusive. In attempting to compare fields from two such crack tip regions for possible similarity, what features of the fields (stresses, strains) should be examined, at what near tip locations should the comparisons be made, and just 'how close' should the fields be in order to be considered 'close enough' to justify the characterisation 'similar'? These are not easy questions to answer. In fact, they cannot be answered at all except in the context of the overall fracture mechanics approach. Among the relevant information needed to provide answers to the questions posed above are the micromechanisms of fracture (cleavage, void growth, shear localisation) and, *a posteriori*, the success with which the proposed model truly correlates the cracking!

Despite these complications, much progress has been made in organising elastic–plastic crack tip fields into 'similar' classes. The two-dimensional simplifications of the plane stress and plane strain idealisations provide a major distinction based on the relative magnitudes of out-of-plane fields with respect to in-plane values; the former case is associated with negligible transverse stress and appreciable transverse thinning, while plane strain fields are characterised by the converse. Moreover, within the class of plane strain crack tip fields, there exists a range of local fields which differ appreciably from one another in their in-plane kinematics and in the triaxiality of stress. The high stresses of the most constrained of the plane strain plastic crack tip fields generally lead to the lowest measure of toughness among the family, and much effort has been devoted to understanding and characterising the various plane strain fields and their dependences on crack geometry, loading type, and magnitude, and degree of material strain hardening.

Although all cracked bodies are in reality three-dimensional, the notion of local plane strain conditions prevailing along the crack front (except at isolated points such as the intersection of the crack front with a free surface) has remained a central feature of 3D applications of elastic–plastic fracture. Mathematically, conditions of asymptotic plane strain along three-dimensional crack fronts can be rationalised by postulating singular in-plane strain at locations along the crack front, and further assuming that extensional strain tangent to the crack front (locally out-of-plane) is either bounded or merely of lower order singularity than the in-plane deformation. In either case, the ratio of out-of-plane strain to a norm of in-plane strain vanishes as the crack front is approached, leading to an asymptotic plane strain state of stress. These rather mild conditions, which are fulfilled in linear elastic solutions of buried elliptical cracks and which have been numerically observed in precise linear elastic solutions as well, also seem plausible in elastic–plastic crack problems. Thus, a major theme in 3D elastic–plastic analysis is the interpretation of 3D crack front fields in terms of their similarity to various of the plane strain crack tip fields noted above.

The plan of this paper is as follows. In the next section, we review certain aspects of the phenomenology and characterisation of the various plane strain crack tip fields. Next, we review some detailed aspects of three-dimensional elastic–plastic crack front fields which have recently been obtained, and discuss how these results can be compared with plane strain crack tip fields. One of the problems, tensile loading of a part-through surface-cracked plate with large crack aspect ratio ($a/c = 0.24$), is readily compared with plane strain loading of a single edge notch (SEN) geometry, owing to near plane strain flow in the long, relatively constant depth ligament near midplane. As loading increases, the plane-strain-like fields which are observed along the crack front display decreasing levels of constraint, as inferred from profiles of stress versus distance. The other 3D problem, elastic–plastic deformation along a through crack in a thin ductile plate, principally illustrates how the loss of plane strain constraint comes to alter the crack front fields.

Finally, we briefly discuss possible generalisations of single-parameter (e.g., J-based) and recently proposed two-parameter characterisations of plane strain crack tip fields which could provide a truly three-dimensional perspective on the characterisation of three-dimensional elastic–plastic crack front fields.

Plane strain crack tip fields

HRR fields

In the crack analysis of monotonically loaded bodies undergoing significant non-linear (plastic) deformation in the vicinity of the crack front and (in some cases) over the entire uncracked ligament, it is convenient to consider an 'equivalent' non-linear elastic material model which coincides with the response of the plastic material under conditions of proportional stressing. A fairly general phenomenological power law model of non-linear uniaxial tensile behaviour is

$$\varepsilon = \alpha\varepsilon_0(\sigma/\sigma_0)^n \tag{1}$$

Here ε and σ are strain and stress, respectively, and material parameters are σ_0, an effective yield stress; $\varepsilon_0 = \sigma_0/E$ (E is Young's modulus), a reference yield strain; n, the strain hardening exponent; and α, a dimensionless factor. This relation can be tensorially generalised using J_2 deformation theory plasticity to provide the (plastic) strain, ε_{ij}, as

$$\varepsilon_{ij} = \alpha\varepsilon_0 \tfrac{3}{2}(\sigma_e/\sigma_0)^{n-1} s_{ij}/\sigma_0 \tag{2}$$

where s_{ij} is the stress deviator, and $\sigma_e = \sqrt{(3s_{ij}\, s_{ij}/2)}$ is the von Mises equivalent tensile stress. Small geometry change asymptotic analysis of a plane strain symmetrically-loaded, mathematically sharp crack tip in such a material leads, as local cylindrical co-ordinate r (measuring distance from the crack tip) approaches zero, to crack tip fields

$$\sigma_{ij}(r, \theta) \to \sigma_0[J/(\alpha\varepsilon_0\, \sigma_0\, I_n\, r)]^{1/n+1} \tilde{\sigma}_{ij}(\theta, n) \equiv \sigma_{ij}^{\mathrm{HRR}} \tag{3}$$

$$\varepsilon_{ij}(r, \theta) \to \alpha\varepsilon_0[J/(\alpha\varepsilon_0\, \sigma_0\, I_n\, r)]^{n/n+1} \tilde{\varepsilon}_{ij}(\theta, n) \equiv \varepsilon_{ij}^{\mathrm{HRR}} \tag{4}$$

Here $\tilde{\sigma}_{ij}$ and $\tilde{\varepsilon}_{ij}$ are dimensionless functions of their arguments, and $I_n(n)$ is a normalising factor. These fields were determined by Hutchinson **(7)** and Rice and Rosengren **(24)**, and are collectively referred to as the HRR singular fields. An extensive tabulation of these fields was given by Shih **(26)**. For fixed material properties, the magnitude of these fields is given solely by the value of the loading parameter J. When the HRR fields truly dominate the complete crack tip fields over large distances compared to crack tip blunting and fracture process zones, it is a natural extension of LEFM methodology to correlate crack extension with J.

The asymptotic fields of equations (3)–(4) do not apply *too* close to the crack tip, since effects of finite geometry change due to blunting have been neglected. An effective crack tip opening displacement (CTOD), δ_t, can be defined from the HRR fields as the crack separation where ± 45 degrees lines emanating from the crack tip intercept the opening crack faces. The resulting value can be expressed, Shih **(25)**, as

$$\delta_t = d_n(\alpha\varepsilon_0, n)\frac{J}{\sigma_0} \tag{5}$$

The coefficient d_n is weakly dependent on $\alpha\varepsilon_0$, but varies from ~ 0.8 for large n to ~ 0.3 for $n = 3$.

Since all crack tip fields possess finite blunting zones which are not accounted for by the small geometry change analysis leading to equations (3)–(4), we should not examine numerical solutions for similarity with the HRR fields at distances from the tip which are small enough to be significantly affected by large deformation. We must instead make comparisons at distances which are at least a few multiples of δ_t, and therein lies the difficulty of too literal an interpretation of equations (3)–(4). At any small but *finite* value of r, the HRR fields can at best be considered as a one-term expansion of the complete crack tip field. The actual fields in zones near but finitely removed from the tip will be affected by the overall loading applied to the crack tip region.

Small-scale yielding

One well-posed boundary value problem which applies to all elastic–plastic plane strain crack tips at vanishingly small applied load is small-scale yielding (SSY). In this boundary layer idealisation, the crack tip plastic zone size is sufficiently small so that the surrounding elastic material can be modelled as an infinite region remotely subject in-plane to the square root stress field of LEFM:

$$\lim_{r\to\infty} \sigma_{ij}(r, \theta) = \frac{K_I}{\sqrt{(2\pi r)}}\, f_{ij}(\theta), \tag{6}$$

where f_{ij} denotes the circumferential variation of the components of the dominant linear elastic crack tip stress field. The elastic–plastic boundary value problem thus defined possesses a similar length scale, $(K_I/\sigma_0)^2$, and the solution fields can be expressed as

$$\sigma_{ij}(r, \theta; n; K_I) = \sigma_0\, \hat{\sigma}_{ij}(r/(K_I/\sigma_0)^2, \theta; n) \equiv \sigma_{ij}^{\mathrm{SSY}} \tag{7}$$

$$\varepsilon_{ij}(r, \theta; n; K_I) = \alpha\varepsilon_0\, \hat{\varepsilon}_{ij}(r/(K_I/\sigma_0)^2, \theta; n) \equiv \varepsilon_{ij}^{\mathrm{SSY}} \tag{8}$$

where $\hat{\sigma}_{ij}$ and $\hat{\varepsilon}_{ij}$ are dimensionless functions of their dimensionless arguments.

In SSY, the remote loading and similar scale can also be phrased in terms of the J-integral by using the elastic identity $K_I^2 = JE'$, where $E' = E/(1-\nu^2)$ is the plane strain tensile modulus and ν is Poisson's ratio.

Small geometry change SSY analyses have been performed by Tracey **(29)**, Parks and Wang **(19)**, and by Betegón and Hancock **(3)**. Figure 1, taken from Wang **(30)**, illustrates that the SSY tensile stress distribution just ahead of the crack tip generally lies slightly below the HRR distribution, with increasing deviation associated with higher strain hardening (lower n values). The asymptotic form of the SSY stress fields satisfies $\sigma_{ij}^{\mathrm{SSY}} \to \sigma_{ij}^{\mathrm{HRR}}$ as $r \to 0$. The curves fit to the distributions in Fig. 1 are purely empirical formulae which match the computed results in the range $\sim 0.0002 \leq r/(K_I/\sigma_0)^2 \leq 0.03$; no attempt has been made to incorporate the asymptotic behaviour.

The SSY stress is within 10 percent of the HRR stress fields at all distances $r \leq 0.008J/\alpha\sigma_0\,\varepsilon_0$ for $n = 10$.

Modified boundary layer formulation

Since small-scale yielding is also an asymptotic condition, it is clear that at finite loading of a *finite* plane strain body having crack length a, remaining ligament c, etc., the SSY similarity fields equations (7)–(8) can exist at radius R from the tip only if R/a and R/c are sufficiently small. Since the plastic zone size in SSY is given by $r_p^{\mathrm{SSY}} \doteq \frac{1}{6}(K_I/\sigma_0)^2$, the attainment of crack tip fields

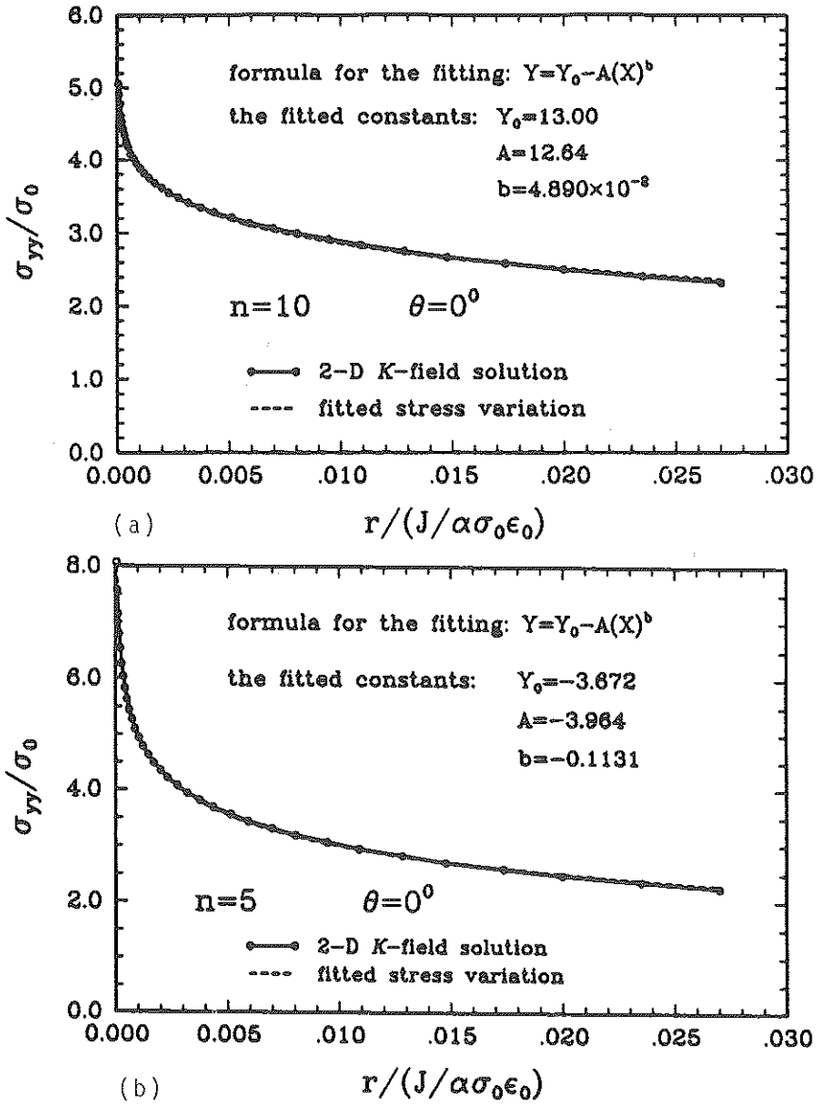

Fig 1 (a) Normalised crack opening stress in plane strain small-scale yielding for hardening exponent $n = 10$. (b) Same curve for $n = 5$ (30).

similar to those of SSY conditions strictly limits the magnitude of applied loading. One way to extend the range of plane strain crack tip fields which are well characterised by *two* loading parameters is the modified boundary layer (MBL) formulation introduced by Rice **(23)**, and by Larsson and Carlsson **(9)**.

In this case, the loading imparted to the crack tip by the surrounding elastic domain is modelled by the first two terms of the elastic Williams **(33)** eigen-expansion:

$$\lim_{r\to\infty}\begin{bmatrix}\sigma_{11}(r,\theta) & \sigma_{12}(r,\theta)\\ \sigma_{21}(r,\theta) & \sigma_{22}(r,\theta)\end{bmatrix}=\frac{K_I}{\sqrt{(2\pi r)}}\begin{bmatrix}f_{11}(\theta) & f_{12}(\theta)\\ f_{21}(\theta) & f_{22}(\theta)\end{bmatrix}+\begin{bmatrix}T & 0\\ 0 & 0\end{bmatrix} \tag{9}$$

Here the 'T' stress component represents a plane strain tension/compression stress parallel to the crack. Rice **(23)** and Larsson and Carlsson **(9)** showed how the MBL formulation could account for differences among a group of specimen geometries in the size and shape of computed plane strain plastic zones loaded to the ASTM E-399 limit of $K_I^2 = 0.4\sigma_0^2 a$. Recently, Bilby *et al.*, **(4)** used non-hardening finite geometry change analysis to show that the stress state deep within the plastic zone can be substantially changed from that of SSY (which corresponds to $T = 0$) by the presence of modest levels of T/σ_0. In particular, negative values of T were found to reduce triaxial stress levels ahead of the crack. Betegón and Hancock **(3)** demonstrated the effects of the T-stress in small geometry change solutions employing power law strain hardening. Like Bilby *et al.*, they noted only slight elevations of stress at any normalised distance for $T > 0$. However, for $T < 0$, they found a nearly uniform decrease (independent of $r/(J/\sigma_0)$) in the crack opening stress at $\theta = 0$. They give the following two-parameter fit to the crack opening stress profile for negative T:

$$\frac{\sigma_{22}^{\mathrm{MBL}}(r;J,\tau)}{\sigma_0}=\frac{\sigma_{22}^{\mathrm{SSY}}(r/(J/\sigma_0))}{\sigma_0}+A_n\tau+B_n\tau^2 \tag{10}$$

where $\tau \equiv T/\sigma_0$ and A_n and B_n are constants dependent on the strain hardening exponent n. The constants are given as $(A_n, B_n) = (0.64, -0.4)$ for $n = 13$, and as $(0.6, -0.75)$ for non-hardening material (formally, $n \to \infty$).

Large-scale yielding

In cases of large-scale yielding in plane strain, the crack tip fields have long been known to display a broad range of triaxiality and kinematics. The variety of fields has been found to be sensitive to several factors, including degree of strain hardening and the crack tip constraint of the fully plastic flow field. This dependence is particularly evident at high n values. In the non-hardening case, McClintock **(11)** demonstrated a broad range of fully plastic crack tip stress and strain-increment states. For centre-cracked plates under plane strain tension, low crack tip constraint is obtained from the straight ± 45 degrees sliplines extending to the free surface, while predominant bending of sufficiently deep edge-cracked geometries leads to crack tip triaxiality similar to the high-n limit of equation (3) or equation (7).

Finite element studies by McMeeking and Parks **(13)** and by Shih and German **(28)** provided quantitative insight into conditions under which the

asymptotic fields of the sort equations (3)–(4) or equations (7)–(8) likely dominate the crack tip region for plane strain geometries such as centre-cracked tension, and edge-cracked bend and mid-ligament tension specimens. These studies provided guidance as to requirements on specimen geometry, loading type and magnitude, and degree of material strain hardening such that the actual crack tip fields are, in fact, 'similar' to the highly-constrained HRR or SSY fields, and therefore are adequately described by the single loading parameter J. For relatively deep cracks, the requirement for sustaining single-parameter plane strain crack tip fields can be compactly expressed in terms of ligament length c and loading amplitude as

$$\mu \equiv \frac{c}{J/\sigma_0} \geqslant \mu_{cr} \tag{11}$$

where μ_{cr} is a 'critical' lower limit. In shallow edge-cracked geometries, equation (11) can be modified into the requirement $a/(J/\sigma_0) \geqslant \mu_{cr}$ (Al-Ani and Hancock **(2)**). Since J increases with load magnitude, equation (11) can alternatively be interpreted as limiting the load which can be applied to a specimen of given material and geometry so that single-parameter crack tip fields are still obtained.

For low hardening materials, it has been found that $\mu_{cr} \simeq 25$ for deep edge cracks in bending. This relatively small value of μ_{cr} means that J-dominance is maintained through fully plastic conditions in this type specimen. McMeeking and Parks **(13)** tentatively suggested that for predominant ligament tension, as in centre-cracked plates, $\mu_{cr} \simeq 200$. This larger value of μ_{cr} effectively limits loading of these geometries to contained yielding. Shih **(27)** has shown that for fully plastic loading of sufficiently deep edge cracks, μ_{cr} varies smoothly, with the ratio of tension to bending, between these values.

Among the recurring problems in efforts to establish limits assuring J-dominance of the crack tip is the fact that, in those geometries which clearly deviate from dominance at fully plastic conditions, the stress fields *gradually* change from the J-dominated ones of SSY as loading increased, and the (implicitly binary) judgement of 'dominated' or 'not' is highly arbitrary. This difficulty can be alleviated by instead characterising the evolution of the crack tip field among a suitably defined 'family' of fields as load is increased.

Recently Al-Ani and Hancock **(2)** have examined the near tip crack opening stress profiles in plane strain edge-cracked geometries of various depths subject to remote tension or bending loads ranging from SSY through fully plastic conditions. At the lowest loadings, local fields were very close to those of SSY (although for some cases, the maximum allowable size of r_p in comparison to crack length was exceedingly small). At load levels corresponding to MBL conditions, the T-stress effects noted in the MBL analyses of Betegón and Hancock **(3)** were observed. Remarkably, both works found that various MBL opening stress profiles given by equation (10) could be accurately fitted to the complete stress fields (over distances $\sim 2\delta_t \leqslant r \leqslant \sim 20\delta_t$) in each of the

specimens and at each load level. Moreover, the two-parameter 'fit' was in each case achieved, based on the actual level of J as determined by, e.g., virtual crack extension, and on a T/σ_0 value linearly proportional to load magnitude, *even up to fully plastic conditions*. That is, the linear elastic T-calibration for the crack geometry and loading type under consideration provided the additional parameter required to specify the particular member of the MBL family of opening stress profiles which fit the actual stress profile. While this is to be expected at loads within the MBL regime, the successes of this simple load parametrisation at load levels corresponding to large-scale yielding and fully plastic situations are difficult to explain. Hancock and co-workers note the curious coincidence that planar crack configurations exhibiting negative T-stress in their linear elastic solutions also tend to have low triaxial crack tip constraint in the corresponding plane strain plastic slip-line solution; the converse is also observed. In any event, the range of plane strain crack geometries, T-stress calibrations, loading types, and load magnitudes for which Hancock and co-workers have successfully demonstrated the accuracy of the two-parameter description of crack opening stress in the region just outside the blunting zone is compelling.

As Al-Ani and Hancock **(2)** note, the not-well-defined requirement of 'J-dominance' which was sought by McMeeking and Parks **(13)** and by Shih and German **(28)** is just the special case of $\tau \geqslant 0$ in the two-parameter characterisation. The profound implications for fracture mechanics methodology of a robust two-parameter characterisation scheme for plane strain elastic–plastic crack tip fields can hardly be overestimated. For example, fracture initiation could perhaps be experimentally identified with a *locus* in the (J, τ) loading space, rather than with a single 'critical' value of J.

Three-dimensional elastic–plastic crack front fields

The understanding of corresponding necessary conditions for HRR-dominance in three-dimensional crack configurations typically encountered in engineering practice remains slight. Brocks and Olschewski **(5)** provided non-linear finite element studies of three-dimensional crack configurations along with certain assessments of HRR-dominance, but the mesh fineness used was far less than in the two-dimensional studies cited. Parks **(18)**, in analysing results from a simple elastic–plastic line-spring model of a part-through surface crack under remote tension, noted that the fully plastic load state at centre-plane tended toward the relatively unconstrained case of mid-ligament tension, likely implying a loss of HRR-dominance. Indeed, recent experimental results by Epstein *et al.* **(6)**, which have been numerically analysed in detail by Wang *et al.* **(32)**, support this contention.

Another three-dimensional situation in which the highly constrained plane strain HRR-type crack front fields can be lost at sufficiently high loads is the case of a straight through-crack of length a in a plate of thickness t, especially

under tensile loading. The important three-dimensional geometrical parameters in such a body are t/a, t/w (where in-plane specimen width is $w = a + c$, and c is uncracked ligament) as well as (in-plane) relative crack depth a/w. Elastic–plastic crack front fields in general depend on all of these ratios, in addition to the dependencies on loading type and magnitude noted above. The parametric complexity of this class of problems has precluded complete study. However, one case which has been analysed in some detail is (in-plane) SSY in a thin plate, Nakamura and Parks **(15)**. The geometric requirements of their idealisation are that $t/a \ll 1$ and that both a/w and c/w are likewise very small. 'Small' loads were considered, so that the three-dimensional extent of crack front yielding always satisfied $r_p/L \ll 1$, where L denotes any characteristic in-plane dimension such as a, c, etc. Accordingly, loading was described in a three-dimensional boundary layer fashion, enforcing equation (6) for the remote in-plane stress components, $\sigma_{\alpha\beta}$, with the understanding that this zone was in a state of plane stress. Plastic zone growth was monitored over load levels ranging from $r_p/t \ll 1$ to $r_p/t \gg 1$. As the plastic zone and crack front blunting zone radially expanded, they entered a region where there was negligible plane strain constraint against transverse thinning, and local crack front fields in the range $\sim 2\delta_t \leqslant r \leqslant 10\delta_t$ began to deviate appreciably from equations (3)–(4). At any load, deviation was greatest near the free surface, diminishing toward mid-plane.

In this section, we will briefly highlight these two studies as idealised modes of alteration of local crack front fields from HRR-type constraint.

Computational procedures

Computations were performed using the small displacement gradient formulation in version 4-6-162 of the ABAQUS finite element program on individual processors of an Alliant FX-8 computer. A deformation theory elastic–plastic Ramberg–Osgood material model was used, with strain hardening exponents $n = 10$ (low hardening) and $n = 5$ (high hardening). Typical solution times for each iteration were of the order of 60 minutes for models of order 11 000 degrees of freedom.

Global equilibrium (in the virtual work sense) was enforced by stringent tolerances on acceptable nodal force imbalances. The maximum permissible force imbalance was of order $10^{-3} \times \sigma_0 l^2$, where l is a characteristic linear dimension of the crack tip elements. Due to the non-linear elastic nature of the constitutive model, this tolerance was typically met in three global iterations per increment, and quadratic convergence was exhibited.

J-values along the crack front were determined using the virtual crack extension (VCE) method (Parks **(16)**), as modified in version 4-6 of ABAQUS following the work of Li *et al.* **(10)** and Nakamura *et al.* **(14)**. Evaluation of J from computations performed over various domains is available. Experience has shown that domain independence in the computed J values can be an

indicator of the overall accuracy of the calculations. In all cases, J values obtained from 6 domains agreed, for each crack front location, to within 4 percent.

Local stress values were sampled at both the reduced Gauss points and from extrapolations to the nodal points.

Tensile-loaded surface-cracked plates

Geometries and loadings

Parks and Wang **(19)** and Wang *et al.* **(32)** analysed wide plates under remote uniaxial tension of magnitude σ^∞ normal to a centrally-located part-through surface crack. The plates had thickness t, total width $2b$, and total length $2h$. The surface cracks considered were semi-elliptical in shape, with maximum penetration a and total surface length $2c$. Figure 2 shows one-quarter of the structural geometry, including the global coordinates (X, Y, Z). In the post-processing of the data obtained near the crack front, local co-ordinates (x, y, z), indicated in the figure, were used. In addition, the parametric angle ϕ locating positions along the semi-elliptical crack front given by $(X/c)^2 + (Z/a)^2 = 1$ is shown, where $X = c \sin \phi$ and $Z = a \cos \phi$. The local z-axis is tangent to the crack front, and the local y-axis, which coincides with the global Y-axis, is normal to the crack plane. In the local co-ordinate system, cylindrical coordinates (r, θ) are given by $r = \sqrt{(x^2 + y^2)}$ and $\theta = \arctan(y/x)$.

The geometrical ratios chosen for the plate were $b/t = 8$ and $h/t = 16$. The crack depths considered were moderately deep, near halfway through. A semi-circular crack front (denoted SC) had $a/t = 0.5$ and $a/c = 1$. A semi-elliptical crack front (denoted SE) had $a/t = 0.6$ and $a/c = 0.24$. These specific ratios were chosen to match the experimental geometries used by Epstein *et al.* **(6)**.

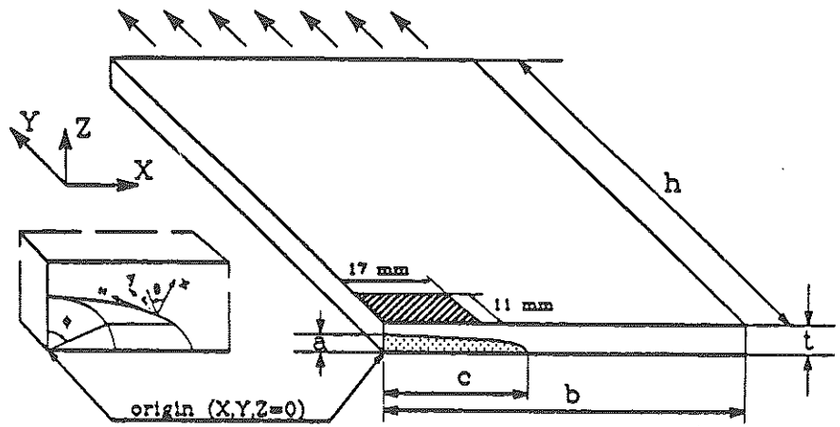

Fig 2 Schematic view of one-fourth of a surface-cracked plate subject to remote tension, showing global coordinates (X, Y, Z) and local co-ordinates (x, y, z) along a semi-elliptical crack front. Crack front position parameter ϕ is also indicated (Wang *et al.* (32))

In simulation of the loading imparted to the reduced thickness portion of their specimens, uniform displacements U_Y were applied at the remote boundary, $Y = h$. The symmetry conditions $U_X = 0$ on $X = 0$ and $U_Y = 0$ on the portion of the plane $Y = 0$ exterior to the crack were also imposed.

The resulting finite element solutions were essentially in a state of uniform remote tension, although an extremely small through-thickness gradient, due to the eccentric location of the crack, could be discerned in the far field. This effect was neglected in the data reduction, and the loading was taken to be characterised by the average remote stress, $\sigma^\infty \equiv P/2bt$, where P is the total load applied to the complete specimen. In practice, P was obtained from the nodal reaction forces imposing the remote displacement.

Finite element meshes

An automatic finite element mesh generator, Wang **(30)**, was used to construct moderately refined global meshes for both crack geometries. Reduced integration ($2 \times 2 \times 2$ Gaussian) 20-node isoparametric brick elements were used. Focused onto each of 12 segments (equal increments in ϕ) of the crack front were 8 degenerate wedge-shaped elements. In the topological element 'plane' locally normal to the crack front, 6 rings of focused elements extended from the crack front to the boundary of a rectilinear subset of the specimen (full thickness). In applying boundary conditions on the degenerate elements having independent nodes located at the same point on the crack front, the region was treated as the limiting case of a keyhole-shaped crack front of vanishing root radius.

Each global mesh had 834 elements, 4345 nodes, and 13 035 degrees of freedom. The radial extent (local r direction) of the crack front elements in the global meshes was roughly $0.02t$. At lower remote loads, this was too large to accurately resolve the local fields over distances of order J/σ_0, where equations (3)–(4) might be expected to apply. Consequently, refined meshes, consisting of 'tubular' regions surrounding the crack front, were developed. The exterior of the fine mesh coincided with the interelement boundary between the third and fourth rings of focused elements in the respective coarse meshes. The fine mesh had 3897 nodes, 768 elements, and 11 691 degrees of freedom. Loading of the fine mesh was accomplished by applying the nodal displacements obtained from the coarse mesh solution. The propriety of this procedure was determined by comparing the stress fields, nodal reaction forces, J values, *etc.* in the two solutions.

Results

Figures 3(*a*) (SE) and 3(b) (SC) show normalised centre plane ($\phi = 0$) local J values versus the normalised load parameter $\Sigma^\infty \equiv \sigma^\infty/\sigma_0$. Each figure contains results for both strain hardening exponents. At low stress, $\Sigma^\infty \leqslant \sim 0.5$, the two curves coincide, and J is essentially the elastic value K_I^2/E'. Linear elastic J calculations (not shown) were typically within 5 percent of those given by Raju and Newman **(30)**. At intermediate stress levels,

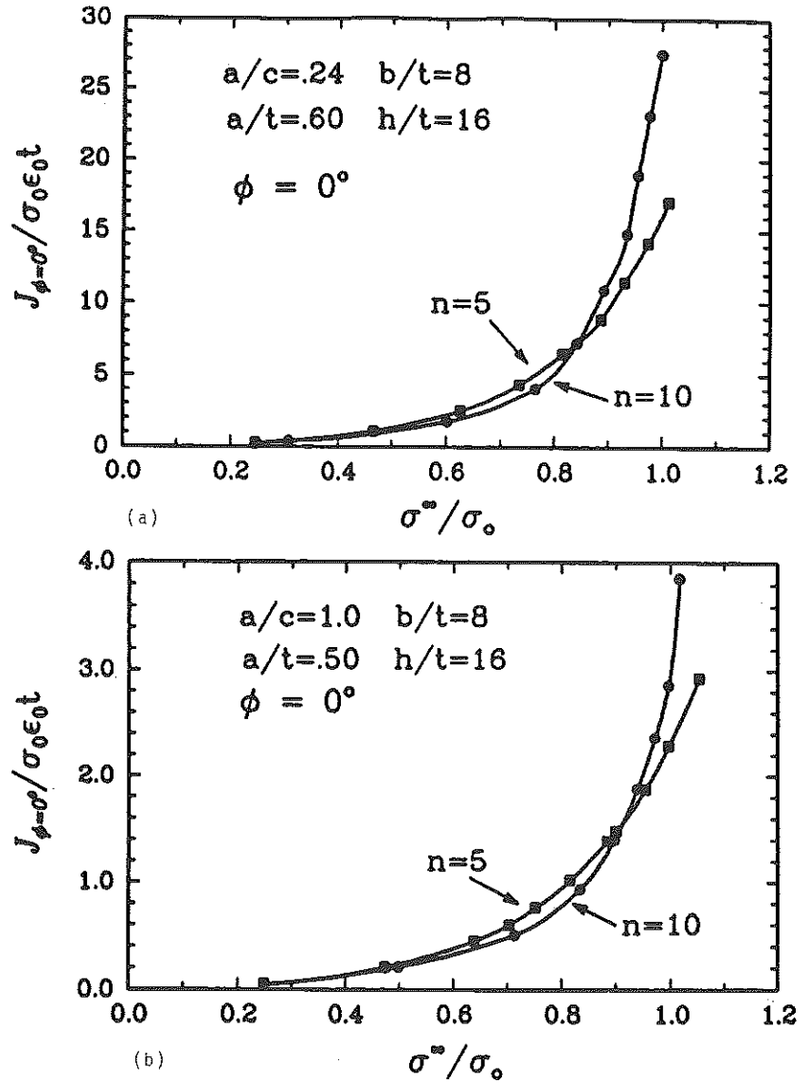

Fig 3 (a) Normalised centre-plane J-value versus normalised load amplitude for SE surface crack geometry in materials with hardening exponents $n = 10$ and $n = 5$. (b) Same curves for surface cracks of SC geometry (Parks and Wang (19))

$0.5 \leqslant \Sigma^\infty \leqslant \sim 0.9$, the J-values from the $n = 5$ curves are slightly greater than those for $n = 10$. At higher stress values, the rapid increase of J in the $n = 10$ material is evident.

Figure 4 shows that the *shape* of the distribution of J^{local} along the crack front in these problems is relatively insensitive to stress level and degree of

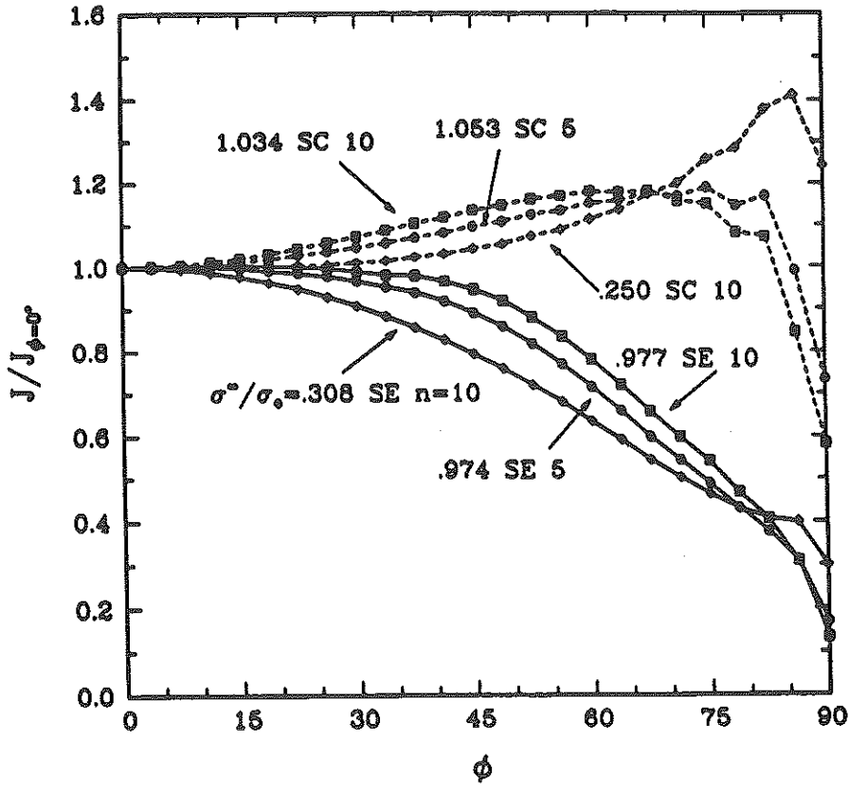

Fig 4 Normalised *J*-distributions along the crack fronts of the tensile-loaded surface-cracked specimens of SE and SC geometries, at various load levels and for both $n = 10$ and $n = 5$. The three-part notation for each curve denotes normalised applied stress (Σ^∞), crack geometry (SE or SC), and strain hardening exponent ($n = 10$ or 5), respectively. Regardless of load level or hardening exponent, the *shapes* of the *J*-distributions in both of the specimen geometries are similar (Parks and Wang (19))

strain hardening. Three curves of $J(\phi)$, normalised by centre plane ($J_{\phi=0}$) values, are shown versus ϕ for both the SE and SC geometries. At the lowest load level shown for each geometry, the distribution is essentially the same as the linear case (Raju and Newman **(20)**). Even at fully plastic conditions, $\Sigma^\infty \sim 1$, the shape of each geometry's normalised *J*-distribution has changed very little. *J*-distributions at intermediate stress levels, not shown for purposes of clarity, essentially interpolate the small distance between elastic and fully plastic curves for both the SE and SC geometries. Thus, Figs 3–4 permit the evaluation of J^{local} at any point along either crack front in either material at any load level shown.

As a check on the coarse mesh/fine mesh re-analysis procedure, the J^{local} values were obtained from the VCE method as applied to both meshes. Results were indistinguishable at lower load levels, with a maximum pointwise

difference less than 4 percent at the highest load. This agreement was acceptable.

Parks and Wang **(19)** examined the opening displacements of the crack surfaces very near the crack front. The value of crack tip opening displacement constructed from the ± 45 degrees intercept method was compared with the asymptotic result of equation (5). This portion of their study was motivated by the trends shown by McMeeking and Parks **(13)**, who noted that the slopes of δ_t versus J curves in different plane strain specimen geometries of the same material model, while coinciding with asymptotic values at low loads, generally diverged in the fully plastic regime. In the 3D surface-cracked specimens, however, no marked divergence of local δ_t versus J curves was observed at any point along either crack front geometry in either material and at any load. Indeed, results were universally within 5 percent of that given by equation (5). The only exceptions which should be noted are the crack openings at the intersection of the crack front and the free surface ($\phi = 90$ degrees). At these locations, the slopes of the δ_t versus J curves were steeper than that given by the plane strain version of equation (5). These results are likely due to both the enhanced near surface deformation associated with the loss of plane strain-like constraint, as well as limitations of the current grids in accurately resolving J^{local} values and their gradients in the near-surface region.

Wang *et al.* **(32)** compared the computed crack opening profiles for the SE geometry with experimental values obtained by Reuter and co-workers **(21)** at load levels near $\Sigma^\infty = 0.93$, just prior to stable tearing. These local CTOD profiles, shown in Fig. 5, are in very good agreement. The experimental values were obtained from metallographic sectioning of unloaded specimens and from fracture surface topography of companion specimens broken in liquid nitrogen after unloading from an applied load near $\Sigma^\infty = 0.93$. The top curve estimates CTOD from equation (5), using the computed J^{local} at the load level $\Sigma^\infty = 0.955$. The circle data is from the ± 45 degrees intercept definition as applied to the finite element solution at the same load. The estimated profile for an 'unloaded' finite element solution was made by subtracting $d_n(\Delta K_I)^2/2\sigma_0 E'$ from the computed δ_t at load. Here ΔK_I is the elastically-calculated change in stress intensity factor on unloading from $\Sigma^\infty = 0.955$ to $\Sigma^\infty = 0$. The doubled yield stress, $2\sigma_0$, was suggested by Rice **(22)**. The calculated δ_t distributions shown in Fig. 5 are based on large geometry change analysis, which was performed to account for pronounced global rotations of the surface-cracked specimen at loads in the fully plastic regime. However, the small geometry change solutions of Parks and Wang **(19)** gave $J(\phi)$ and $\delta_t(\phi)$ profiles close to the calculations of Wang *et al.* **(32)**, and to the experiments of Epstein *et al.* **(6)**.

Local stress state

Parks and Wang **(19)** compared the computed crack opening stress component, σ_{yy}, directly ahead of the crack front ($\theta = 0$) with the plane strain SSY fields of equation (7) for each material. The stress at any point was normalised

The points furthest from the crack tip are the first to feel the strong effects of interaction with the external plastic flow fields, while the nearer points begin to be affected only at somewhat higher loads. Still, regardless of the distance chosen, it is clear that substantial deviation from HRR-dominance is felt at centre plane in this problem near $\Sigma^{\infty} = 0.9$.

Plots like that shown in Fig. 7 can illustrate and quantify the effects of other variables, including crack aspect ratio and degree of strain hardening, on both the initially gradual and ultimately abrupt loss of HRR/SSY J-dominance. Figure 8 compares the decrease of normalised local stress with increasing Σ^{∞} at various locations along the SE and SC crack fronts, for the case of $n = 10$. The distance from the crack front at which each curve is drawn is $r = 6\delta_t$. While this distance is somewhat arbitrary, it is clear from Fig. 7 that very similar results would be obtained for other plausibly relevant distances. The SC geometry is more resistant to abrupt loss of HRR-dominance in the fully plastic regime than is the SE configuration. The decrease from HRR/SSY J-dominance continues to be essentially linear along the semi-circular crack front up to $\Sigma^{\infty} = 1.04$. The trend of decreasing dominance with decreasing ϕ is also followed in this crack geometry (over the range $\phi < \sim 60$ degrees; i.e., regions not too close to the intersection of crack front and free surface at $\phi = 90$ degrees). The marked difference in fully plastic J-dominance displayed by these two crack geometries is due to the relative ease with which deformation can focus into plane-strain-like behaviour. Once the surrounding material reaches flow conditions, the long, relatively constant depth ligament near the centre of the SE geometry readily accommodates the lightly constrained in-plane flow typical of a single edge crack under tension. In contrast, the minimum ligament depth and crack front radius of curvature are equal in the SC geometry, and no such planar modes of flow are available. Hence, relative HRR-dominance is retained to higher stress levels in the SC geometry. Indeed, experimental evidence consistent with this conclusion has been provided by Epstein *et al.* **(6)**, as has computational evidence by Wang *et al.* **(32)**.

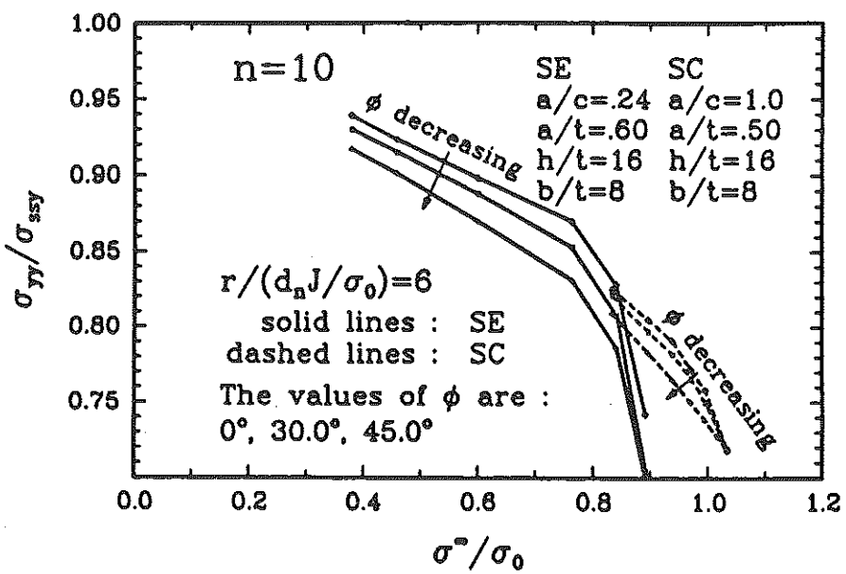

Fig 8 Normalised crack opening stress at $r = 6\delta_t$ ahead of the crack front, versus normalised load, for various crack front locations in the SC and SE surface-cracked geometries in specimens with hardening exponent $n = 10$ (Parks and Wang (19))

Figure 9 shows the effect of strain hardening level on the retention and loss of HRR-dominance. For the SE geometry, local normal stress, normalised by σ_{yy}^{SSY}, is plotted versus Σ^{∞}. Curves are shown at three crack front locations in materials with $n = 5$ and $n = 10$. Again, the distance from the crack tip at which the comparison is made is $r = 6\delta_t$. The trend of decreasing dominance with decreasing ϕ is evident in both materials, but the higher hardening material ($n = 5$) shows both higher overall magnitudes of normalised local stress, and less susceptibility to abrupt loss of dominance at fully plastic conditions. At the highest applied stress, the divergence from dominance is accelerating in the high-hardening material. Thus, the higher hardening may only delay the rapid loss of J-dominance to Σ^{∞}-levels perhaps 15 percent greater than in low-hardening materials.

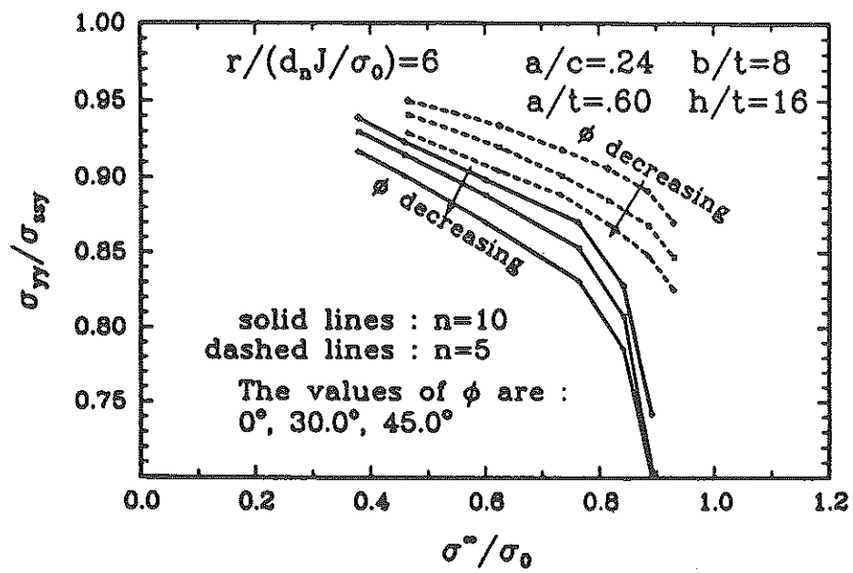

Fig 9 Normalised crack opening stress at $r = 6\delta_t$ ahead of the crack front, versus normalised load, for various crack front locations in the SE surface-cracked geometry specimens with hardening exponents of $n = 10$ and $n = 5$ (Parks and Wang (19))

SSY in a thin three-dimensional plate

Geometry and loading

The geometry of the problem considered by Nakamura and Parks **(15)** is shown in Fig. 10. A circular disc containing the crack tip in a large thin plate (a) was removed, modelling the near tip region as in (b). The straight crack front was located at the centre of the disc along the z-axis ($x, y = 0$). Only a quarter of the disc (region $0 \leqslant \theta \leqslant \pi$, $0 \leqslant z/t \leqslant 1/2$) was modelled. The radial extent of the disc was $r_{max} = 100t$, where the in-plane K_I displacement boundary conditions

$$u_\alpha = \frac{K_I}{E}\, g_\alpha(\theta, \nu)\sqrt{\frac{r}{2\pi}} \tag{12}$$

were applied uniformly across the thickness. The far-field load is thus characterised by $J^{far} \equiv K_I^2/E$. The problem contains two characteristic dimensions, thickness (t) and $J^{far}/\sigma_0 \varepsilon_0$, and length dimensions can be normalised with these two scales.

Nakamura and Parks **(15)** found strong three-dimensionality within $r \leqslant t/2$, a 3D → 2D transition region comprising the annulus $t/2 \leqslant r \leqslant 3t/2$, and essentially plane stress conditions for $r \geqslant 3t/2$ at all levels of applied loading. The degree of plane strain constraint, as reflected by the parameters $\sigma_{zz}/(\sigma_{rr} + \sigma_{\theta\theta})$ and $|\varepsilon_{zz}|/\varepsilon_e$ (where ε_e is equivalent tensile strain), was invariably higher near mid-plane than near the lateral traction-free surface at all in-plane coordinates (r, θ).

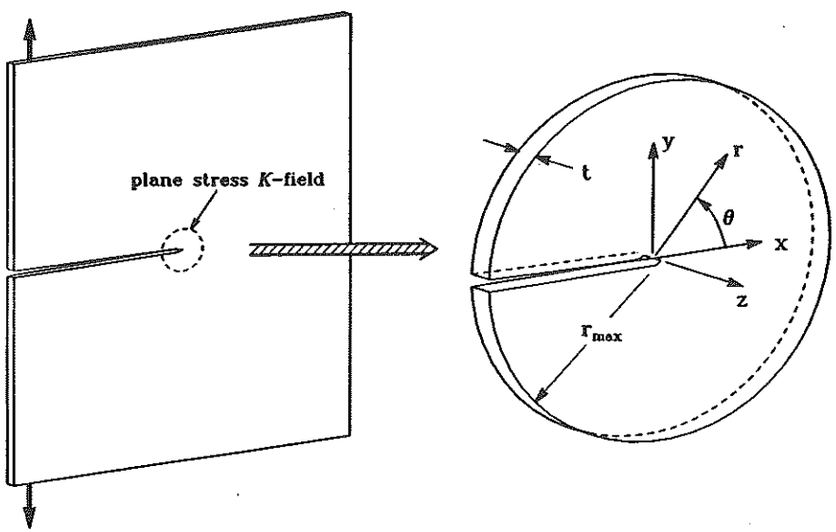

Fig 10 (a) Schematic of a thin plate subject to symmetrical remote loading. A boundary of a region assumed to be dominated by a plane stress K_I field is indicated. (b) Near-crack-front region of a thin plate represented by a circular disc. Cartesian and cylindrical co-ordinates are indicated (Nakamura and Parks (15))

J and CTOD

For the case of $n = 10$, the local J value, J^{local}, normalised by J^{far}, is plotted versus z/t in Fig. 11 for several load levels. The arc-length weighted average of J^{local} differed from J^{far} by less than 2 percent, in agreement with in-plane SSY.

CTOD profiles were calculated from the ± 45 degrees intercept definition at each load level, assuming $\alpha = 1$ and $\varepsilon_0 = 1/300$. The opening displacements at various positions z/t along the crack front were normalised with J^{local}. Results are shown as functions of remote load level in Fig. 12, along with the plane strain HRR asymptotic estimate of equation (5). At low loads, the normalised δ_t approaches the HRR limit at all crack front locations except very near the free surface. A nearly constant $\delta_t/(J^{local}/\sigma_0)$ is observed within $|z/t| \leqslant 0.354$ under a wide range of load level. However, as in the surface crack studies, the agreement of the ratio of local δ_t to J^{local} with that of the HRR solution does not assure HRR-dominance of the local fields.

Local stress and deformation fields

For the mid-plane location, Fig. 13 shows the degree of local plane strain constraint, and the associated effect on the crack opening stress, as a function

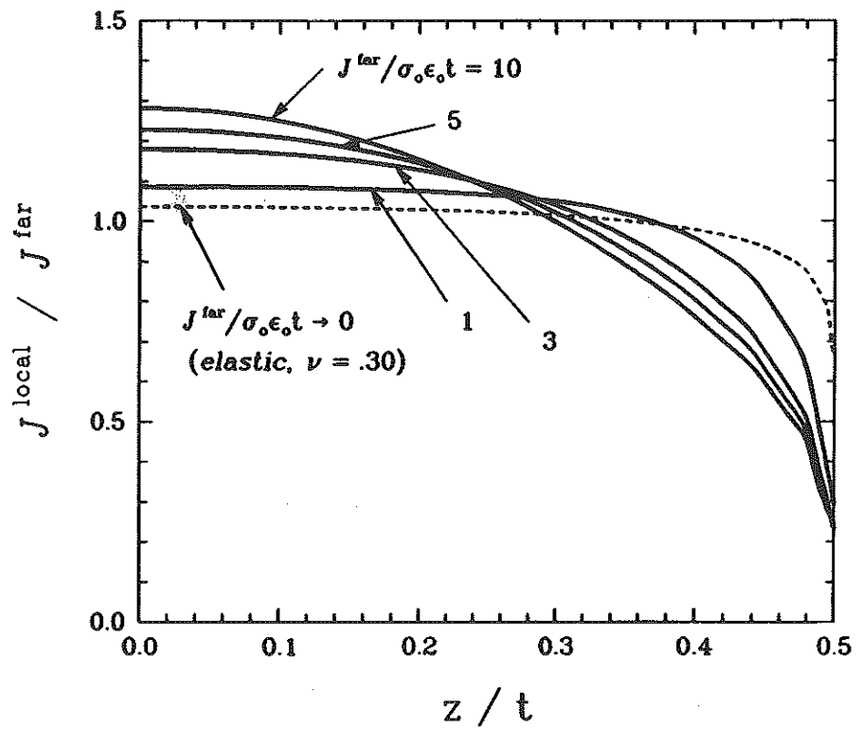

Fig 11 Distribution of J^{local}, normalised by J^{far}, along the crack front of a thin ductile plate under various levels of 'in-plane' small-scale yielding (Nakamura and Parks (15))

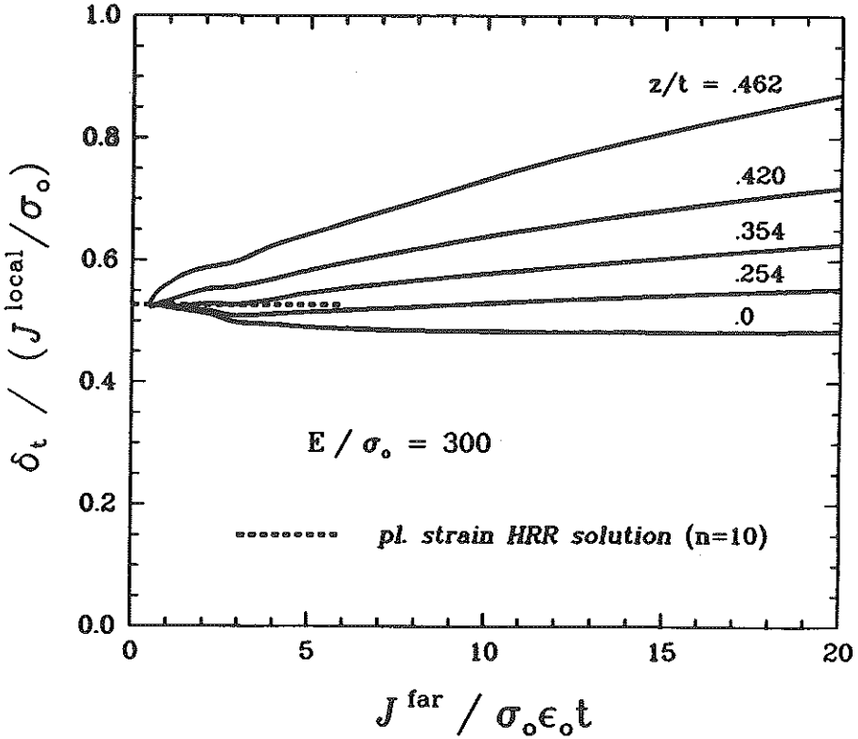

Fig 12 Normalised crack tip opening displacement versus load amplitude at various planes normal to the crack front of a thin ductile plate subject to in-plane small-scale yielding (Nakamura and Parks (15))

of distance from the crack front normalised by $J^{\text{local}}/\sigma_0$. Results are shown for several values of remote load amplitude, $J^{\text{far}}/\sigma_0\,\varepsilon_0\,t$. In Fig. 13(a), the transverse strain is normalised by $\varepsilon_{\max}$, which is the largest equivalent strain for any point a distance r from the tip, according to the HRR field of equation (4). In Fig. 13(b), the opening stress is represented by the hoop stress $\sigma_{\theta\theta}$ at $\theta = 5$ degrees, and it is normalised by the corresponding component of the plane strain SSY field, equation (7). For reference, the outer boundary of the neglected finite geometry change region, $r \simeq 3\delta_t$, is located near 1.5 on the abscissa, assuming $\alpha\varepsilon_0 = 1/300$. At the lowest load of $J^{\text{far}}/\sigma_0\,\varepsilon_0\,t = 1$, the out-of-plane contractional strain is less than 2 percent of the (in-plane) HRR equivalent strain over most of the small geometry change region, and the stress profile agrees well with SSY. As load magnitude increases, the out-of-plane deformation becomes increasingly important, relative to HRR-based in-plane strain levels, and the local opening stress profiles display a corresponding deviation from SSY. The trends indicated in this figure for the mid-plane location occur more strongly for crack front locations nearer the free surface;

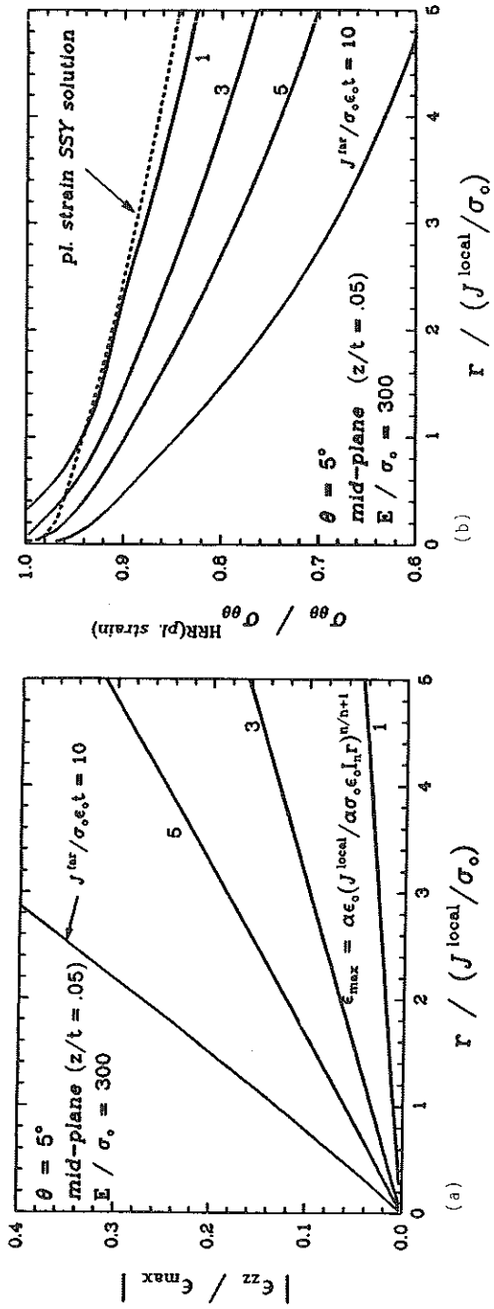

Fig 13 (a) Normalised tangential strain at mid-plane of a thin ductile plate subject to in-plane small-scale yielding, plotted versus normalised distance ahead of the crack tip, for various levels of applied loading. The normalising strain measure $\varepsilon_{\max}(r)$ is the maximum equivalent tensile strain occurring a distance r from a plane strain crack tip, according to the HRR field, equation (4). (b) Normalised crack opening stress at mid-plane of a thin ductile plate, plotted versus normalised distance ahead of the crack tip, for various levels of applied loading. Also shown is the curve for plane strain small-scale yielding, equation (7)

levels of deviation similar to those shown at mid-plane in Fig. 13 are evident at lower values of $J^{far}/\sigma_0\,\varepsilon_0\,t$ for crack front locations nearer $z = t/2$.

Discussion

The examples given in the preceding section illustrate some of the effects which can be observed in three-dimensional elastic–plastic crack front fields. Can an effective framework, analogous to the two-parameter MBL-based description of plane strain crack tip fields proposed by Hancock and co-workers, be developed for three-dimensional crack front fields as well?

As a first attempt to apply the MBL-type approach to a three-dimensional problem, consider the form which can be obtained by manipulation of equation 10, which can be rewritten as

$$\frac{\sigma_{22}^{MBL}(r;\,J^{local},\,\tau)}{\sigma_{22}^{SSY}(r/(J^{local}/\sigma_0))} = 1 + \frac{A_n\tau + B_n\tau^2}{\sigma_{22}^{SSY}/\sigma_0} \tag{13}$$

In a three-dimensional body such as the semi-elliptical surface-cracked plate, an elastic analysis of a *local* T-type stress expansion coefficient would scale proportionally with remote stress: $T = \sigma^{\infty}\cdot\hat{t}$, where $\hat{t}$ is a constant depending on crack front location and overall geometry. Dividing the notional T-stress correlation by σ_0, and recalling the definitions $\tau = T/\sigma_0$ and $\Sigma^{\infty} = \sigma^{\infty}/\sigma_0$, provides $\tau = \Sigma^{\infty}\cdot\hat{t}$. On substituting this relation into equation (13), there obtains

$$\frac{\sigma_{22}^{MBL}(r;\,J^{local},\,\tau)}{\sigma_{22}^{SSY}(r/(J^{local}/\sigma_0))} = 1 + \frac{A_n\hat{t}\Sigma^{\infty} + B_n(\hat{t}\Sigma^{\infty})^2}{Y_0 - A(\alpha\varepsilon_0\,\sigma_0\,r/J^{local})^b} \tag{14}$$

where the denominator of the term on the right side of equation (14) is the empirical fit to the SSY stress profile shown in Fig. 1. The functional form of equation (14) is indeed approximately that shown by the normalised stress versus load curves of Figs 7–9. At low loads, $\Sigma^{\infty} < \sim 0.8$, a reasonable fit to the curve in Fig. 7 at the distance $r = 6d_n\,J^{local}/\sigma_0$ is obtained by simply setting $\hat{t} \doteq -0.60$ in equation (14). (In making this estimate, the Betegón–Hancock parameters A_n and B_n were linearly extrapolated in terms of $1/n$ to $1/n = 1/10$.) This purely 'curve-fitting' value for $\hat{t}$ has been confirmed in two independent ways. Wang and Parks **(34)** have also obtained an approximate centreplane value of $\hat{t} = -0.6$ from a line-spring analysis of this geometry, while highly refined 3D linear elastic analysis of the crack front provides the improved estimate $\hat{t} = -0.65$ (Wang and Parks **(34)**), which, when inserted into equation (14), provides a slightly better fit to the computed stress profiles.

This exercise was intended only to motivate the following three-dimensional generalisation of the MBL formulation. Consider a section of crack front in a three-dimensional body which has traction-free crack faces. Let the local normal to the crack plane be the local x_2 direction, with local crack front tangent direction x_3. The following generalisation of equation (9) would seem to be a natural way to express higher order aspects of the linear elastic stress

distribution in the vicinity of the crack front location:

$$\lim_{r\to 0}\begin{bmatrix}\sigma_{11} & \sigma_{12} & \sigma_{13}\\ \sigma_{21} & \sigma_{22} & \sigma_{23}\\ \sigma_{31} & \sigma_{32} & \sigma_{33}\end{bmatrix} = \frac{K_I}{\sqrt{(2\pi r)}}\begin{bmatrix}f_{11}(\theta) & f_{12}(\theta) & f_{13}(\theta)\\ f_{21}(\theta) & f_{22}(\theta) & f_{23}(\theta)\\ f_{31}(\theta) & f_{32}(\theta) & f_{33}(\theta)\end{bmatrix} + \begin{bmatrix}T_{11} & 0 & T_{13}\\ 0 & 0 & 0\\ T_{31} & 0 & T_{33}\end{bmatrix} \tag{15}$$

where the constant stress state T_{ij} is in general a complete local plane stress state leaving the crack face traction-free. On certain symmetry planes, the constant shear stress term can be argued to vanish: $T_{13} = 0$. The plane strain MBL formulation corresponds to the special case $T_{13} = 0$ and $T_{33} = \nu T_{11} \equiv \nu T$. It would seem that the three bounded, non-zero terms T_{11}, T_{33}, and T_{13}, should independently be considered as capable of altering the local crack front fields from the plane strain SSY distribution. Indeed, recent results by Wang **(31)** confirm that both T_{11} and T_{33} must be considered in accurately describing the near-front 3D elastic–plastic fields. Rigorous formulation of the 3D-MBL formulation requires that plasticity be truly contained. In order that the constant remote asymptotic 3D field T_{ij} does not violate a von Mises yield criterion (based on σ_0 as yield stress), it is necessary that

$$\sigma_0 > \sqrt{(T_{33}^2 - T_{11}T_{33} + T_{11}^2 + 3T_{13}^2)} \equiv T^e \tag{16}$$

where T^e is the equivalent stress corresponding to T_{ij}. This requirement of course applies to computational formulations of the plane strain MBL formulation as well. In practice, MBL plastic zone sizes can grow as large as $T^e \to \sigma_0$, requiring some care in modelling in order to achieve the postulated remote boundary conditions. In the absence of T_{11} and T_{13}, the tangential stress of a 3D-MBL formulation is limited to $|T_{33}| < \sigma_0$, corresponding to a limiting remote tangential strain of (at most) $|E_{33}| < \varepsilon_0$. The tangential strain E_{33} is applied uniformly in a generalised plane strain model (ABAQUS **(1)**) of 3D-MBL conditions, Wang **(31)**. Thus, the magnitude of loss of transverse plane strain constraint which can be strictly accounted for within the 3D MBL formulation is quite limited in comparison with the effects noted in Fig. 13(a). Consequently, the magnitude of the changes in normalised stress opening profile which are achievable are less than those observed in Fig. 13(b), especially in the regime $3\delta_t \leqslant r \leqslant 6\delta_t$, although rather large alterations from SSY can be obtained for $r > \sim 10\delta_t$.

The kinematic deviations from plane strain constraint which can occur (see Fig. 13(a)) are considerably larger. For example, at a load of $J^{far}/\sigma_0\,\varepsilon_0\,t = 3$, the mid-plane tangential strain at $r = 3d_n\,J^{local}/\sigma_0$ is $\simeq -0.05\varepsilon_{max}$, where the latter parameter is understood to be evaluated at the same distance. Assuming $\alpha\varepsilon_0 = 1/300$ and $n = 10$, gives $d_n = 0.53$, $I_n = 4.54$, and $\varepsilon_{max} = 0.098$. Thus, $\varepsilon_{33} = -0.005 \simeq -1.5\varepsilon_0$. At this level of loss of crack front plane strain constraint, shifting of the opening stress profile beneath the SSY results is seen at distances from the front of the order $3\delta_t$. Perhaps some sort of kinematical

second parameter such as $\mathscr{E} \equiv E_{33}/\varepsilon_0$ could be incorporated into a three-parameter description of crack front fields. Of course, the 3D solution of the thin plate noted above doubtless possesses local in-plane T-stress values, of the sort considered by Betegón and Hancock **(3)**, which must be taken into consideration in a more complete analysis.

Whether or not some 3D generalisation of the formalism can be extended to load levels beyond the rigorous limits of the MBL formulation, as Hancock and co-workers have demonstrated for the two-parameter plane strain MBL characterisation, remains to be seen. In view of the two 'prototypical' modes by which local 3D elastic–plastic crack front fields have been demonstrated to deviate from HRR- or SSY-type constraint, some such robust categorisation of local fields would be very desirable.

Acknowledgements

This work was supported by the Office of Basic Energy Sciences, Department of Energy, under Grant # DE-FG02-85ER13331. Computations were performed on an Alliant FX-8 computer obtained under D.A.R.P.A. Grant # N00014-86-K-0768 and on a Data General MV-10000 computer donated to M.I.T. by the Data General Corporation. The ABAQUS finite element program was made available under academic licence from Hibbitt, Karlsson, and Sorensen, Inc., Providence, RI.

I am pleased to acknowledge useful interactions and discussions with several individuals, including Y.-Y. Wang. T. Nakamura, J. W. Hancock, and J. G. Merkle.

References

(1) ABAQUS USER'S MANUAL (1987) Verion 4–6, Hibbitt, Karlsson, and Sorensen, Inc., Providence, Rhode Island.
(2) AL-ANI, A. M. and HANCOCK, J. W. (1989) J-dominance of short cracks in tension and bending, Glasgow University Report, to appear, *J. Mech. Phys. Solids.*
(3) BETEGÓN, C. and HANCOCK, J. W. (1989) Two-parameter characterisation of elastic–plastic crack tip fields, Glasgow University Report, to appear, *J. App. Mech.*
(4) BILBY, B. A., CARDEW, G. E., GOLDTHORPE, M. R., and HOWARD, I. C. (1986) A finite element investigation of the effect of specimen geometry on the fields of stress and strain at the tip of stationary cracks, *Size Effects in Fracture*, Inst. of Mech. Engrs, London, 37–46.
(5) BROCKS, W. and OLSCHEWSKI, J. (1986) On J-dominance of crack-tip fields in largely yielded 3D structures, *Int. J. Solids and Structures*, **22**, 693–708.
(6) EPSTEIN, J. S., LLOYD, W. R., and REUTER, W. G. (1988) Three-dimensional CTOD measurements of elastic–plastic surface flaws, *Analytical, Numerical, and Experimental Aspects of Three-Dimensional Fracture Processes*, (Edited by A. J. Rosakis, *et al.*), ASME AMD-91, American Soc. of Mech. Engrs, New York, 33–50.
(7) HUTCHINSON, J. W. (1968) Singular behaviour at the end of a tensile crack in a hardening material, *J. Mech. Phys. Solids*, **16**, 13–31.
(8) HUTCHINSON, J. W. (1983) Fundamentals of the phenomenological theory of nonlinear fracture mechanics, *ASME J. of App. Mech.*, **50**, 1042–1051.
(9) LARSSON, S. G. and CARLSSON, A. J. (1973) Influence of non-singular stress terms and specimen geometry on small-scale yielding at crack tips in elastic–plastic material, *J. Mech. Phys. Solids*, **21**, 263–278.

(10) LI, F. Z., SHIH, C. F., and NEEDLEMAN, A. (1985) A comparison of methods for calculating energy release rate, *Engng Fracture Mech.*, **21**, 405–421.
(11) McCLINTOCK, F. A. (1971) Plasticity aspects of fracture, *Fracture: an Advanced Treatise*, **III**, (Edited by H. Leibowitz), Academic Press, New York, 47–225.
(12) McMEEKING, R. M. (1977) Finite deformation analysis of crack-tip opening in elastic–plastic materials and implications for fracture, *J. Mech. Phys. Solids*, **25**, 357–381.
(13) McMEEKING, R. M. and PARKS, D. M. (1979) On criteria for J-dominance of crack tip fields, *Elastic–Plastic Fracture*, (Edited by J. D. Landes, *et al.*), ASTM STP *668*, pp. 175–194, ASTM, Philadelphia.
(14) NAKAMURA, T., SHIH, C. F., and FREUND, L. B. (1989) Three-dimensional transient analysis of a dynamically loaded three-point-bend ductile fracture specimen, *Nonlinear Fracture Mechanics: I – Time-Dependent Fracture*, ASTM STP *995*, p. 217, ASTM, Philadelphia.
(15) NAKAMURA, T. and PARKS, D. M. (1989) Three-dimensional crack front fields in a thin ductile plate, MIT Report of Research in the Mechanical Behavior of Materials, to appear, *J. Mech. Phys. Solids.*
(16) PARKS, D. M. (1977) The virtual crack extension method for nonlinear material behavior, *Computer Methods in Appl. Mech. Engng*, **12**, 353–364.
(17) PARKS, D. M. (1980) The dominance of the crack tip fields of inelastic continuum mechanics, *Numerical Methods in Fracture Mechanics*, (Edited by D. R. J. Owen, and A. R. Luxmoore), Pineridge Press, Swansea, U.K., 239–260.
(18) PARKS, D. M. (1981) The inelastic line-spring: estimates of elastic–plastic fracture mechanics parameters for surface-cracked plates and shells, *ASME J. Pressure Vessel Technology*, **103**, 246–254.
(19) PARKS, D. M. and WANG, Y.-Y. (1988) Elastic–plastic analysis of part-through surface cracks, *Analytical, Numerical, and Experimental Aspects of Three-Dimensional Fracture Processes*, (Edited by A. J. Rosakis, *et al.*), ASME AMD-91, American Society of Mech. Eng., New York, 19–32.
(20) RAJU, I. S. and NEWMAN, J. C. Jr. (1979) Stress intensity factors for a wide range of semi-elliptical surface cracks in finite-thickness plates, *Engng Fracture Mech.*, **11**, 817–829.
(21) REUTER, W. G. (1988) private communication to D. M. Parks.
(22) RICE, J. R. (1967) Mechanics of crack tip deformation and extension by fatigue, *Fatigue Crack Propagation*, ASTM STP *415*, pp. 247–309, ASTM, Philadelphia.
hia, 247–309.
(23) RICE, J. R. (1974) Limitations to the small-scale yielding approximation for crack tip plasticity, *J. Mech. Phys. Solids*, **22**, 17–26.
(24) RICE, J. R. and ROSENGREN, G. F. (1968) Plane strain deformation near a crack tip in a power law hardening material, *J. Mech. Phys. Solids*, **16**, 1–12.
(25) SHIH, C. F. (1981) Relationships between the J-integral and the crack opening displacement for stationary and extending cracks, *J. Mech. Phys. Solids*, **29**, 305–326.
(26) SHIH, C. F. (1983) Tables of Hutchinson–Rice–Rosengren singular field quantities, Brown University Report, MRL E-147.
(27) SHIH, C. F. (1985) J-dominance under plane strain fully plastic conditions: the edge crack subject to combined tension and bending, *Int. J. Fracture*, **29**, 73–84.
(28) SHIH, C. F. and GERMAN, M. D. (1981) On requirements for a one-parameter characterisation of crack tip fields by the HRR singularity, *Int. J. Fracture*, **17**, 27–43.
(29) TRACEY, D. M. (1976) Finite elements for crack-tip behavior in small-scale yielding, *ASME J. Engng Mat. Tech.*, **98**, 146–151.
(30) WANG, Y.-Y. (1988) Analysis of fracture initiation in surface cracked plates, *M. Sc. Thesis*, Depart. Mech. Engng, Massachusetts Institute of Technology.
(31) WANG, Y.-Y. (1989) Ph.D. research, in progress.
(32) WANG, Y.-Y., PARKS, D. M., LLOYD, W. R., REUTER, W. G., and EPSTEIN, J. (1989) Elastic–plastic deformation in surface-cracked plates: experiment and numerical analysis, MIT Report of Research in the Mechanical Behaviour of Materials, *J. Appl. Mech.*, in press.
(33) WILLIAMS, M. L. (1957) On the stress distribution at the base of a stationary crack, *ASME J. App. Mech.*, **24**, 111–114.
(34) WANG, Y.-Y. and PARKS, D. M. (1990) Evaluation of the elastic T-stress in surface-cracked plates using the line-spring method, MIT Report of Research in the Mechanics of Materials, submitted for publication.